CHAPTER 5

Critical behavior at the smectic-*A* to smectic-*C*, nematic to smectic-*A* and isotropic to nematic phase transitions in a binary pyrimidine liquid crystal mixtures from high-resolution optical birefringence measurement

5.1. Introduction

Classical liquid crystal phases are characterized by broken symmetries and may be utilized to explore the complex and beautiful relationship in nature between symmetry and spatial dimensionality at phase transitions. The smectic layers are characterized by a quasi-long range one dimensional mass-density wave along the ***z***-direction (*i.e.*, parallel to the layer-normal) and by a director (local orientational axis) which can either be parallel to the ***z***-axis (Sm-*A*) or at an angle inclined to the ***z***-axis (Sm-*C*). The transition between the Sm-*A* and Sm-*C* phases involves the breaking of a continuous rotational symmetry. Proposing the order parameter associated with the Sm-*A*–Sm-*C* transition to be $\psi = \theta \exp(i\phi)$, where θ is the tilt angle of the director with respect to the smectic layer normal and ϕ is an azimuthal angle, de Gennes has predicted that the Sm-*A*–Sm-*C* phase transition is continuous and should exhibit the same critical behavior as the superfluid transition in helium, *i.e.*, this transition should belong to the $d = 3$, $n = 2$ universality class (3D-*XY* model) [1]. However, the deviations from the helium-like behavior have often been observed in close vicinity of that transition [1-10]. A large number of experimental results from heat-capacity measurements have demonstrated classical mean-field behavior and can be described in the context of the extended mean-field model including the terms up to sixth-order in the tilt order parameters [2-8]. There are also several examples in which the heat capacity shows Landau behavior including tricritical appearance [9,10], while in some other cases, clear deviation from the mean field character has been observed, revealing either a 3D-*XY* or Gaussian tricritical behavior or a crossover from 3D-*XY* to tricritical nature [11-16]. The ultrasonic velocity and birefringence measurements have also been found to yield frequently non-Landau outcomes [17-20]. For butyloxy-benzylidene-heptylaniline (4O.7), it has been observed that the measurements of the tilt-angle variation face the difficulty of distinguishing critical behavior from mean field character on the

basis of order-parameter data alone, whereas the heat capacity and tilt-susceptibility data are uniquely described by the mean-field Landau model [4,5]. Therefore, the question that arises is why certain compounds show mean-field behavior while others critical behavior. Such a discrepancy is perhaps due to the fact that the bare correlation length describing the tilt fluctuations is usually much large so that the true critical region is unobservably small [21] and it may become inaccessible in certain experimental techniques. Later, Benguigui and Martinoty [22] tried to solve this issue using the Ginzburg criterion and proposed that the true critical behavior is expected only when $|\tau|<\tau_G$, where τ is the reduced temperature and τ_G is the Ginzburg temperature. They claimed that width of the critical region linked with the Sm-*A*–Sm-*C* phase transition is dependent on the physical properties studied, and consequently may lead to varying outcomes for the dissimilar observables probed. As in the ultrasonic velocity measurements, the elastic constants are found to exhibit non-Landau nature for their more sensitivity to fluctuation effects than the other measurement methods like heat capacity [22]. Safinya *et al.* showed that due to the large bare correlation lengths, as obtained from x-ray studies [21], the Ginzburg criterion yields $\tau_G \sim 10^{-5}$. Since the Sm-*C* ordering is apparently not driven by long-range interaction and the Sm-*A*–Sm-*C* transition is not at or above the upper critical dimensionality ($d = 4$ for the *XY* universality class), mean-field theory is not applicable for the exact representation of this transition [23]. However, Huang and Lien [24] and Prasad *et al.* [25] indicated the possibility of observing a first-order or tricritical behavior of this transition by reduction of the Sm-*A* temperature range. Therefore, the absolute nature of the Sm-*A*–Sm-*C* phase transition (*i.e.*, its universality class) is still not properly been understood and necessitates further measurements, appropriate for studying the pretransitional fluctuation at this transition.

In chapter 3, the experimental verification of the crossover phenomena from 3D-*XY* to tricritical behavior by decreasing the nematic (*N*) temperature range has been found to be quite successful in the *N*–Sm-*A* phase transition [26,27]. Therefore, it is quite plausible to expect that occurrence of such crossover from 3D-*XY* to tricritical and thereafter to first-order behavior seems to be related to the width of the Sm-*A* temperature range [24,25]. Thus the discovery of a suitable system that manifests critical fluctuations associated with the Sm-*A*–Sm-*C* transition is very important. Such a situation has been reported for a few phenyl pyrimidine compounds [28] and also in azoxy-4,4-bi-undecyl-*α*-methylcinnamate (AMC-11) [29] as well as some chiral systems [30]. As light is sensitive to the average molecular direction, probably optical measurements are accurate enough to allow for a discussion about the nature of the Sm-*A*–Sm-*C* phase transition. It has been well established in chapter 3 that the birefringence data can suitably be employed to study the critical anomaly at both the *I*–*N* and the *N*–Sm-*A* phase transitions with a reasonably good accuracy. In fact, this method provides considerably precise data for Δn with a good reproducibility near the phase transition and hence facilitating a suitable interpretation of results – critical behavior, which in many cases become not possible in high resolution calorimetric or other measurements. Hence, the birefringence measurement is expected to supply further insights for clarifying whether or not the phase transition is of the Landau mean-field type.

In this chapter, a high-resolution temperature scanning technique has been employed to determine the optical birefringence (Δn) in a pure 5-*n*-heptyloxy-2-(4-*n*-nonyloxy-phenyl) pyrimidine (PhP2, the seventh homolog) liquid crystal as well as in some binary mixtures of the same with the second homologous compound 5-*n*-ethyloxy-2-(4-nonyloxy-phenyl) pyrimidine (PhP1) of the same series, to test the possibility of crossover behavior from nearly tricritical to 3D-*XY* critical nature near the Sm-*A*–Sm-*C* transition by reducing the temperature range of the Sm-*A* phase. Investigations have also

been carried out simultaneously at the nematic–smectic-*A* (*N*–Sm-*A*) phase transitions from which a comparative discussion has been established concerning the similarity and dissimilarity of order nature for both the transitions [31,32]. Additionally, the critical behavior in the vicinity of isotropic–nematic (*I*–*N*) phase transition has been reported for all of the studied mixtures including a pure compound.

5.2. Materials

The materials studied, were synthesized at the Institute of Chemistry, Military University of Technology, Warsaw, Poland (having purity higher than 99.9%), and were used without further purification. The structural formulae and the stable mesophase sequences for both the compounds are given below:

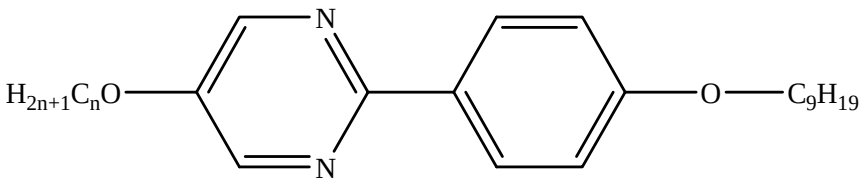

Compound 1: For **PhP1,** n = 2**;** Phase sequence as follows,

Cr (359.7 K) ***N*** (363.5 K) ***I***

Compound 2: For **PhP2,** n = 7**;** Phase sequence as follows,

Cr (330 K) **Sm-*C*** (352.45 K) **Sm-*A*** (363.5 K) ***N*** (367.55 K) ***I***

Eight mixtures of the binary system were prepared by adding small amounts of 5-*n*-ethyloxy-2-(4-nonyloxy-phenyl) pyrimidine (PhP1) compound into the host 5-*n*-heptyloxy-2-(4-*n*-nonyloxy-phenyl) pyrimidine (PhP2) compound having molar concentrations 0.05, 0.1, 0.15, 0.2, 0.3, 0.35, 0.4 and 0.45. The optical textures were observed under a polarizing optical microscope (BANBROS) equipped with HCS302 (INSTEC) hot stage, controlled by mK1000 (INSTEC) thermo system.

5.3. Phase diagram

The partial phase diagram of the binary system consisting of PhP2 with the second compound, PhP1 as obtained from polarizing optical microscopy and the optical transmission technique has been illustrated in Fig. 5.1. The pure compound PhP1 comprises a nematic (*N*) phase appearing in a small range of ~ 3.8 K, but the PhP2 compound exhibit a nematic phase with a temperature range of ~ 4 K along with a Smectic-*A* (Sm-*A*) phase of range ~11 K and a Smectic-*C* (Sm-*C*) phase of range ~ 22 K.

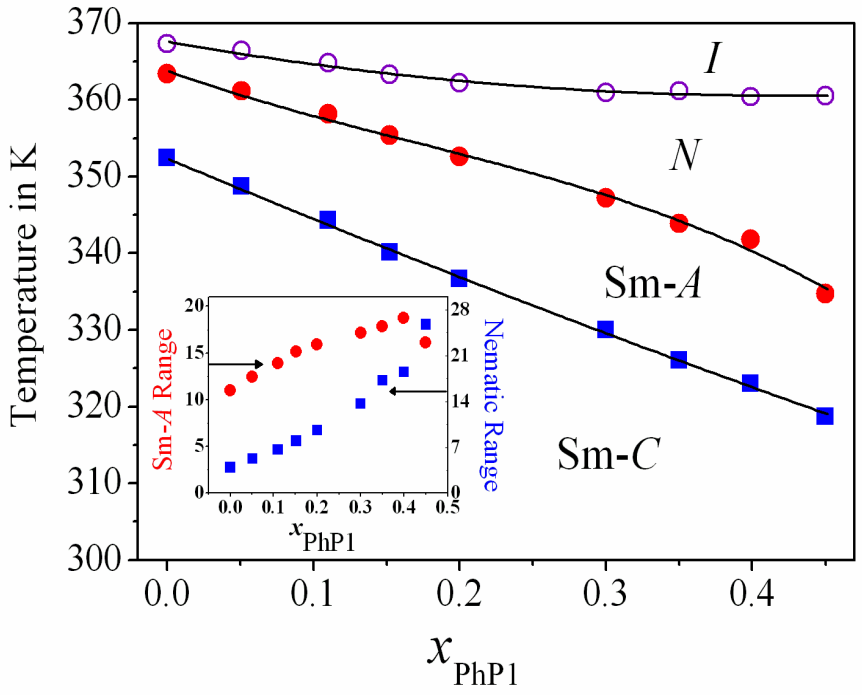

Figure 5.1. Partial phase diagram of the binary system comprising of PhP2 and PhP1. x_{PhP1} denotes the mole fraction of PhP1. *I*– isotropic phase, *N*– nematic phase, Sm-*A*–smectic-*A* phase, Sm-*C*–smectic-*C* phase, ○: isotropic to nematic transition temperature; ●: nematic to smectic-*A* transition temperature; ■: smectic-*A* to smectic-*C* transition temperature; Inset shows the concentration dependence of the Sm-*A* and nematic ranges for the present system. Solid lines are drawn for guidance to eye.

It has been observed that a systematic variation in the *N* and Sm-*A* width has been accomplished by the addition of the second homologue (PhP1) of the same series. The nematic phase range has been found to increase from a value

of 4 K to 27 K whereas the Sm-*A* phase range lies between 11 K and 19 K for the studied mixtures. These variations of the *N* and Sm-*A* ranges against molar concentration is also presented in the inset of Fig. 5.1. The present binary system offers both the variation of *N* and Sm-*A* phase with reasonable ranges, which is very helpful to investigate the order character of the *N*–Sm-*A* and the Sm-*A*–Sm-*C* phase transition simultaneously. Therefore, it is expected that the dependence of the effective critical exponent (α') on the temperature ratios T_{NA}/T_{IN} and T_{AC}/T_{NA} (T_{NA} : *N*–Sm-*A* phase transition temperature, T_{AC} : Sm-*A*–Sm-*C* phase transition temperature, T_{IN} : Isotropic to nematic phase transition temperature) can be investigated more rigorously, thus endowing with the insight on the nature of both the *N* to Sm-*A* and Sm-*A* to Sm-*C* phase transitions from the same binary system of rod-like liquid crystal molecules.

5.4. Optical birefringence measurements

A temperature scanning measurement of the optical birefringence during cooling from isotropic liquid (with the average scanning rate of 0.5 K min^{-1}) to the room temperature have been accomplished by probing the phase retardation ($\Delta\varphi$) of a laser beam (λ = 532 nm) transmitted through a planar aligned ITO coated liquid crystal filled cell of thickness ~7.7 μm [31-37]. The birefringence in the nematic phase was calculated from the measured normalized intensity and this method was extended to the Sm-*A* and Sm-*C* mesophases as well. Moreover, to check the reproducibility of the data, measurements were also performed for several cooling and heating runs and reproducible results were obtained. The variation of optical birefringence (Δn) against temperature (T) for the pure compound (PhP2) and three of the binary mixture having molar concentration x_{PhP1} = 0.1, 0.2 and 0.3 has been represented in Fig. 5.2(a-d). For all of the investigated systems, in the isotropic phase the birefringence value is equal to zero, which on entering the nematic phase increases rapidly following the *I*–*N* phase transition, evidently due to the strong growth of the nematic order. The overall profile of the temperature dependence of Δn is in good

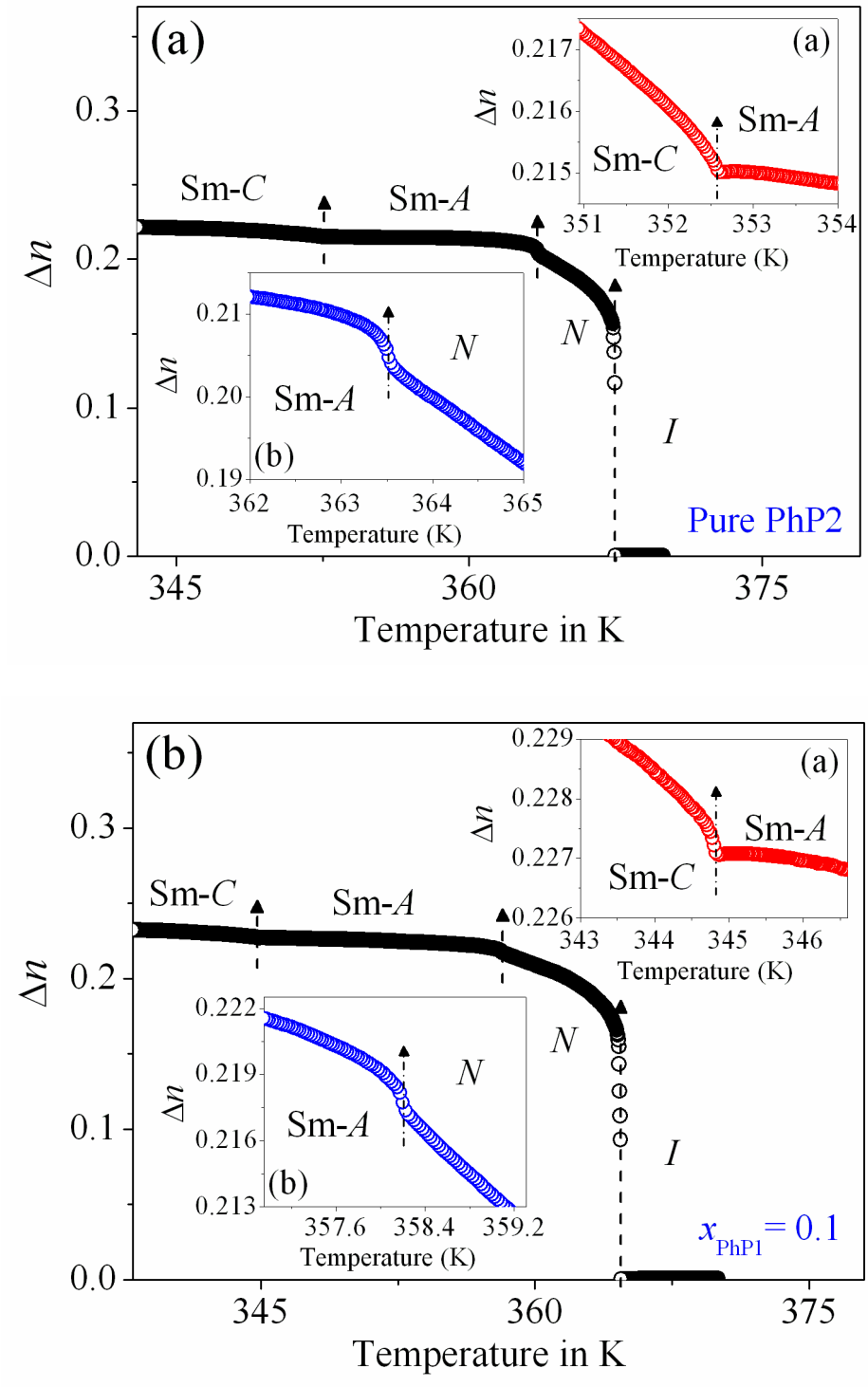

Figure 5.2. Temperature dependence of birefringence (Δn) data for the (a) Pure PhP2 compound and (b) mixture x_{PhP1} = 0.1. Vertical arrows show the *I*–*N*, *N*–Sm-*A* and Sm-*A*–Sm-*C* phase transitions for the mixtures. In the insets variation of birefringence in the vicinity of Sm-*A*–Sm-*C* transition [inset (a)] and *N*–Sm-*A* transition [inset (b)] has been presented.

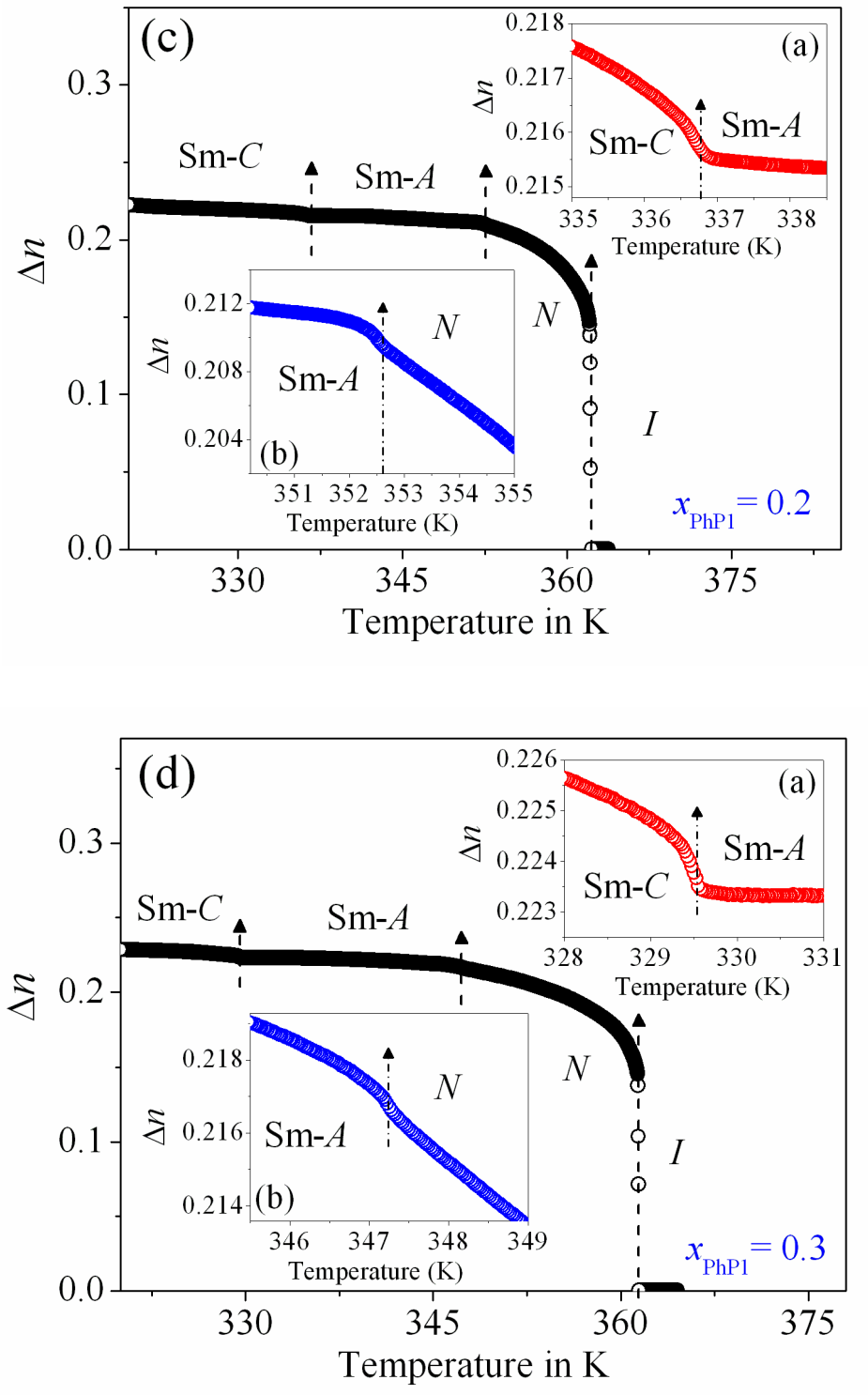

Figure 5.2 (cont'd). Temperature dependence of birefringence (Δn) data for the mixture (c) $x_{PhP1} = 0.2$ and (d) $x_{PhP1} = 0.3$. Vertical arrows show the *I*–*N*, *N*–Sm-*A* and Sm-*A*–Sm-*C* phase transitions for the mixtures. In the insets variation of birefringence in the vicinity of Sm-*A*–Sm-*C* transition [inset (a)] and *N*–Sm-*A* transition [inset (b)] has been presented.

agreement with the reported various rod-like liquid crystals [38]. As seen in Fig. 5.2, upon lowering the temperature towards the Sm-*A* phase, an enhancement in Δn takes place at the *N*–Sm-*A* phase transition. Such augmentation is preferably owing to the smectic-like short-range order, building up within the nematic phase close to the *N*–Sm-*A* phase transition and consequently causing a further enhancement in the nematic (orientational) order. Moreover, on entering the low-temperature tilted Sm-*C* phase there is also a clear and overall increase in Δn due to the Sm-*A*–Sm-*C* phase transition. This may be due to the fact that the molecular long axis in the Sm-*C* phase of the surface aligned (planar cell of thickness 7.7 μm) bulk sample is oriented parallel to the aligning surface and the layers are tilted with respect to the surface alignment which causes an enhancement in the orientational order. Thus, a well-defined Δn curves in the vicinity of the transition temperatures has been obtained. In the present optical technique, the small transitional variation in birefringence and hence the related modification in the mesophase structure can suitably be used to precisely describe the nature of different phase transitions in liquid crystal media.

5.5. Critical behavior at the Sm-*A*–Sm-*C* phase transition

In this study, a sharp increasing nature in the temperature dependence of birefringence data has been observed in going from the Sm-*A* to the Sm-*C* phase. As no visible discontinuity is found in the temperature dependence of Δn at this transition, the exact transition temperature is identified by locating the minimum value of the temperature dependence quantity $[-d(\Delta n)/dT]$. Furthermore, a differential quotient Q(T) has been introduced following the same expression (Eq. 3.6) in Chapter 3 to take a proper look into the critical aspects of the Sm-*A*–Sm-*C* phase transition, defined as [39-41]:

$$\mathrm{Q}(T) = -\frac{\Delta n(T) - \Delta n(T_{AC})}{T - T_{AC}} \tag{5.1}$$

where T_{NA} is changed to T_{AC}, and $\Delta n(T_{AC})$ is the birefringence value at the Sm-*A*–Sm-*C* phase transition temperature (T_{AC}). An overview of the temperature dependent variation of Q(*T*) for pure PhP2, close to the Sm-*A*–Sm-*C* phase transition is shown in Fig. 5.3. The Q(*T*) data exhibit a noticeable anomaly close to that transition, involving an asymmetry between the Q(*T*) wings in the Sm-*A* and Sm-*C* phases. Furthermore, in order to gain an impression of the critical fluctuation in Q(*T*), appearing in the vicinity of the Sm-*A*–Sm-*C* phase transition, fit to the following renormalization group expression has also been performed [41],

$$\mathrm{Q}(T) = \frac{A^{\pm}}{\alpha'}|\tau|^{-\alpha'}(1 + D^{\pm}|\tau|^{\Delta}) + E(T - T_{AC}) + B \qquad (5.2)$$

where, $\tau = (T - T_{AC})/T_{AC}$ is the reduced temperature, α' is the critical exponent similar to the specific-heat capacity critical exponent α and the other parameters are the same as appearing in Eq. (3.7) in Chapter 3, but now they corresponds to the Sm-*A*–Sm-*C* phase transition. The fit to Eq. (5.2) with the measured Q(*T*) data is displayed in Fig. 5.3 as solid line for the PhP2 compound.

In order to realize consistent fittings, few data points very close to the transition have been excluded from the fit process to avoid the error resulting from the experimental uncertainty and sample inhomogeneity. In each fit, the transition temperature was first isolated by identifying the minimum of the temperature dependence of $-d(\Delta n)/dT$ and then was kept fixed. This helps in reducing the instability appearing in the least-squares minimization. The Q(*T*) data exhibit a noticeable divergent character on both side of the transition temperature, involving an asymmetry between the Q(*T*) wings in the Sm-*A* and Sm-*C* phases. In particular, the existence of such divergent behavior above the transition temperature clearly indicates that this transition is not of the mean-field type. It has been observed that the temperature dependence of Q(*T*) data close to T_{AC} is well described by Eq. (5.2), suggesting a good agreement between the experimental optical birefringence data and the theoretical power

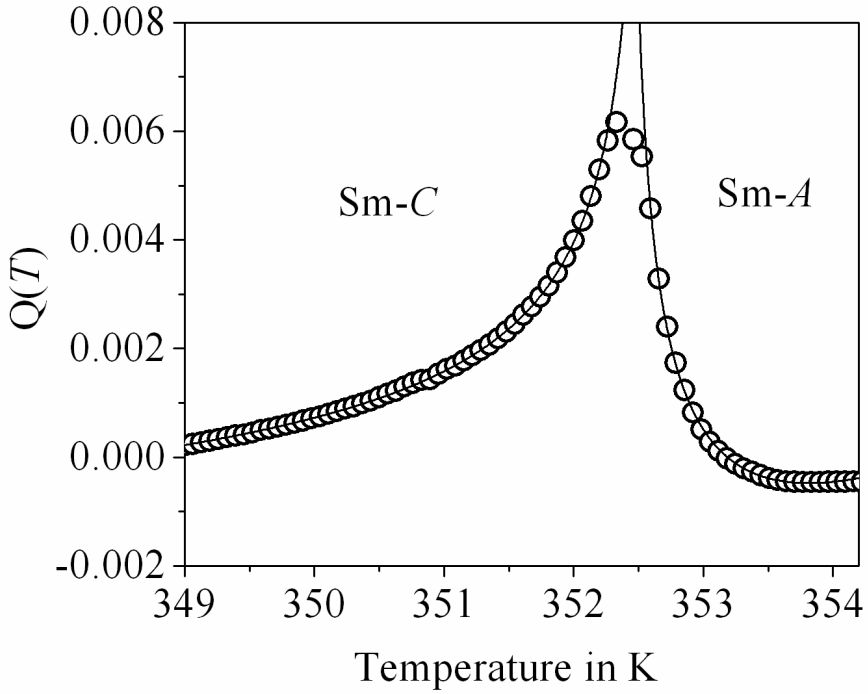

Figure 5.3. The temperature variation of the parameter Q(*T*) near the Sm-*A*–Sm-*C* phase transition. Solid lines are fit to Eq. (5.2) near the Sm-*A*–Sm-*C* phase transition.

Table 5.1. Results corresponding to the best fit for Q(*T*) of pure PhP2 compound near the Sm-*A*–Sm-*C* phase transition obtained in accordance with Eq. (5.2) and related χ_v^2 values associated with the fits. The Sm-*A*–Sm-*C* phase transition temperature T_{AC} = 352.45 K was kept fixed in the fits. $|\tau|_{\max}$ represents the upper limit of reduced temperature considered for these fits.

Phase	α'	A^-, A^+	D^-, D^+	$\lvert\tau\rvert_{\max}$	${\chi_v}^2$
Smectic-*C*	0.478±0.005	0.00031±0.00001	14.4±0.2	3×10^{-3}	1.1
Smectic-*A*	0.474±0.008	0.00024±0.00001	14.2±0.6	3×10^{-3}	1.29
Smectic-*C*	0.477±0.015	0.00016±0.00002	4.4±0.5	5×10^{-3}	1.09
Smectic-*A*	0.483±0.024	0.00014±0.00002	11.4±0.7	5×10^{-3}	1.31
Smectic-*C*	0.488±0.010	0.00013±0.00001	7.3±0.4	1×10^{-2}	1.14
Smectic-*C*	0.502±0.008	0.00011±0.00001	5.7±0.2	1.5×10^{-2}	1.23

law behavior considered. Furthermore, the extracted critical character for the Sm-*A*–Sm-*C* phase transition has usually been found to be sensitive to the width of the temperature range, considered in the fit process. An investigation has been performed herewith to perceive the dependency of fit parameters on the fit range. In the vicinity of Sm-*A*–Sm-*C* transition, fit has been carried out for four different reduced temperature ranges: $|\tau|_{max}$ = 3×10^{-3}, 5×10^{-3}, 1×10^{-2} and 1.5×10^{-2}. Corresponding fit parameters as obtained from the fit process are presented in Table 5.1 for the pure compound. The quality of the fits has been assessed by calculating the related reduced error function χ_v^2 value [42], have been found to be within 1.09 and 1.31 and thus signifying consistent fits. In these fits, the critical exponent (α') for the Sm-*A*–Sm-*C* phase transition depends feebly on the fit range, appeared to be nearly 0.476 and 0.48 for the reduced temperature range $|\tau|_{max}$ = 3×10^{-3} and 5×10^{-3} respectively, yielded slightly higher value for the relatively greater temperature ranges considered. The critical amplitude quotient (A^-/A^+) has been found to be 1.301 and 1.14 for the reduced temperature range $|\tau|_{max}$ = 3×10^{-3} and 5×10^{-3} respectively. However, the D^+ value has been appeared to be comparatively greater than its counterpart in the Sm-*C* phase for $|\tau|_{max}$ = 5×10^{-3} and other higher ranges, thus disagreeing with the theoretical prediction of $D^-/D^+ \sim 1$, while the D^-/D^+ quotient assumes a value 1.01 for the fit range $|\tau|_{max}$ = 3×10^{-3}, which reveals a well consistency with the theoretical value. Such a shortcoming of D^- for the greater fit ranges is perhaps owing to the strong correlation between *D* and *B* and also due to the nearly tricritical character of that transition [43].

Hence, nearly Gaussian (non-classical) tricritical behavior has been revealed for the Sm-*A*–Sm-*C* phase transition of the pure PhP2 compound. Moreover, in the pure compound as the Sm-*A* width is of only 11 K, the unsaturation of the Sm-*A* order parameter close to the Sm-*A*–Sm-*C* phase transition perhaps lead to a large Sm-*C* order correlation length, which also pushes the transition towards a mean-field like character. The dependence of

that transition on the size of the Sm-*A* phase has also been elucidated by others [24,25]. For another pyrimidine liquid crystal, 5-*n*-decyl-2-[4-*n*-(perfluoropentyl-metheleneoxy) phenyl] pyrimidine, with an almost identical Sm-*A* width as the present PhP2 compound, Reed *et al.* also reported a non-Landau, nearly tricritical nature is in line with the observed behavior [28]. However, it has also been observed that the exponent α' demonstrates a weak decrease with the shrinkage of temperature range, considered in the fits. Furthermore, according to Safinya *et al.* as the large correlation length describing the tilt fluctuations results in a highly reduced critical region, experimentally it may not be possible to access the true critical region [21]. Thus there may be a possibility of crossover appearance of the Sm-*A*–Sm-*C* phase transition in this study as the true critical region may be much smaller than the present fit range so that it remains inaccessible. Yet, because of the well-consistency of parameter ratios with the theoretical values and also for revealing a reasonable range of reduced error function χ_v^2, it seems more acceptable to investigate the critical behavior in a range $|\tau|_{max} = 3\times10^{-3}$. However, it is apparent that the critical exponent α' characterizing the critical fluctuations in Q(*T*) is in agreement with the theoretical description based on the renormalization-group method and hence reveal a disagreement of the nature of that transition with the extended Landau mean-field model.

Furthermore, investigation has been carried out for all of the mixtures to observe the dependency of critical exponent (α') with the Sm-*A* phase range. An overview of the temperature-dependent variation of Q(*T*) in the vicinity of Sm-*A*–Sm-*C* phase transition for eight different mixtures including the pure compound is shown in Fig. 5.4 in a fit range $|\tau|_{max} = 3\times10^{-3}$. All of the Q(*T*) data manifesting a divergent behavior on both side of the transition, involving an asymmetry between the Q(*T*) wings in the Sm-*A* and Sm-*C* phases. As both the compounds were chosen from the same homologous series, no Fisher renormalization [44] of the critical exponent has been observed even for nearly

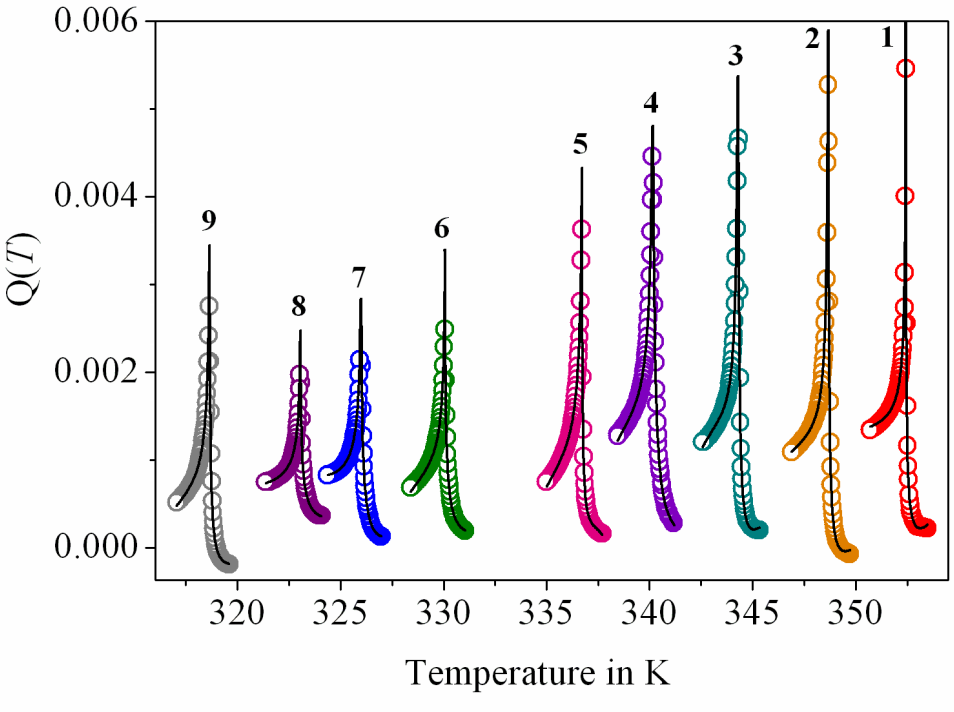

Figure 5.4. The temperature dependence of Q(T) in the vicinity of the Sm-A–Sm-C transition in mixtures of PhP1 and PhP2 for $|\tau|_{max} = 3\times10^{-3}$. 1: $x_{PhP1} = 0.0$; 2: $x_{PhP1} = 0.05$; 3: $x_{PhP1} = 0.1$; 4: $x_{PhP1} = 0.15$; 5: $x_{PhP1} = 0.2$; 6: $x_{PhP1} = 0.3$; 7: $x_{PhP1} = 0.35$; 8: $x_{PhP1} = 0.4$; 9: $x_{PhP1} = 0.45$.

Table 5.2. Results corresponding to the best fit for Q(T) near Sm-A–Sm-C phase transition of all the mixtures obtained in accordance with Eq. (5.2) and related χ_v^2 values associated with the fits.

x_{PhP1}	A^-/A^+	D^-/D^+	α'	χ_v^2
0	1.301±0.001	1.01±0.05	0.476±0.007	1.19
0.05	1.200±0.011	1.00±0.03	0.397±0.006	1.24
0.10	1.080±0.018	0.99±0.05	0.321±0.017	1.17
0.15	1.017±0.098	0.94±0.03	0.237±0.011	1.19
0.20	0.979±0.062	0.93±0.04	0.193±0.007	1.25
0.30	0.911±0.006	0.91±0.03	0.136±0.002	1.13
0.35	0.930±0.002	0.91±0.02	0.089±0.007	1.17
0.40	0.907±0.011	0.91±0.03	0.040±0.006	1.15
0.45	0.936±0.018	0.86±0.06	0.152±0.005	1.08

tricritical compositions. The fits to Eq. (5.2) are displayed as solid lines, while the corresponding fit values are listed in Table 5.2. The reduced error functions χ_v^2, which have been found to be within 1.08 and 1.25, signify consistent fits. However, with increasing the concentration of PhP1 compound, the measured value of critical exponent α' in the vicinity of the Sm-*A*–Sm-*C* phase transition decreases monotonically from 0.476 ± 0.007 for the pure PhP2 compound to 0.04 ± 0.006 for the mixture x_{PhP1} = 0.40, *i.e.*, the yielded values of effective critical exponent α', characterizing the critical fluctuation at this transition, have appeared to be in between those predicted by the 3D-*XY*, *i.e.*, α_{XY} = -0.007 and tricritical, *i.e.*, α_{TCH} = 0.5 values. The variation of the extracted critical exponent (α') values for the present investigated mixtures including pure PhP2 against the temperature ratio (T_{AC}/T_{NA}) is illustrated in Fig. 5.5. Non-universal values have been observed for the critical exponent α' and hence indicate a

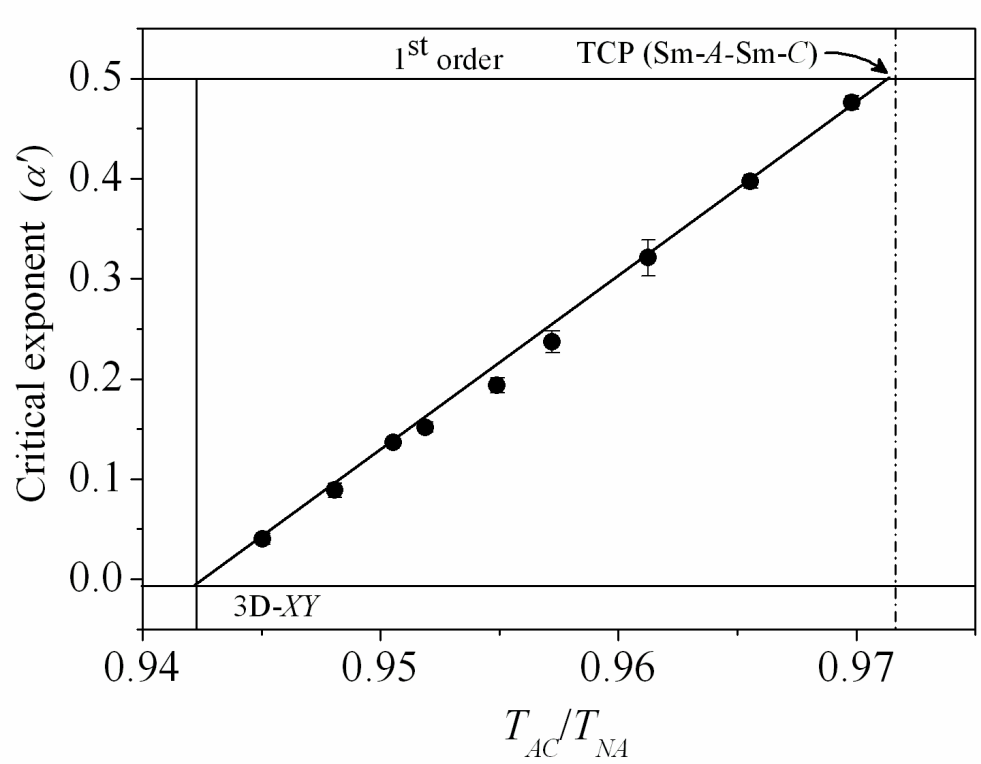

Figure 5.5. Variation of the effective critical exponent (α') with T_{AC}/T_{NA} for Sm-*A*–Sm-*C* phase transition. The vertical dashed line and solid line corresponds to the tricritical point (TCP) and 3D-*XY* limit respectively. The solid line is a linear fit to the data points.

crossover character for the Sm-*A*–Sm-*C* phase transition. An extrapolation of the linear fit to the extracted α' values yield a tricritical point for the T_{AC}/T_{NA} ratio of 0.972 and reveal a T_{AC}/T_{NA} value of 0.942 corresponding to the 3D-*XY* point. It should also be mentioned here that this crossover of α' gives rise to the characteristic behavior regarding amplitude ratio (A^-/A^+) and the magnitude of the first-order corrections-to-scaling terms (D^-/D^+). In that case, the A^-/A^+ values are in the range between 1.301 and 0.907 (from the extrapolation of the linear fit it yields about 1.39 for the tricritical point (TCP) and 0.954 for the 3D-*XY* point) and the first-order corrections-to-scaling ratio is between 1.01 to 0.86 (from the extrapolation of the linear fit it yields about 1.05 for the TCP and 0.89 for the 3D-*XY* point). The theory for the 3D-*XY* universality class predicts an amplitude ratio $A^-/A^+ = 0.971$ and $D^-/D^+ \approx 1$ while for TCP the theoretical amplitude ratio $A^-/A^+ = 1.6$ and $D^-/D^+ \approx 1$. Therefore, from this observation, it is clear that the studied mixtures exhibit non-universal behaviors with effective critical exponents lying between the 3D-*XY* and tricritical limits.

5.6. Critical behavior at the *N*–Sm-*A* phase transition

Following the same procedure as discussed in chapter 3 the critical anomaly associated with the *N*–Sm-*A* phase transition has been explored to the present system as well from the precise Δn data. In this study, similar renormalization group expression including the corrections to scaling term have been reused, in an attempt to obtain an insight into the limiting behavior of the quotient Q(*T*) near the *N*–Sm-*A* phase transition.

The temperature dependence of Q(*T*) for the pure compound PhP2 in the vicinity of *N*–Sm-*A* phase transition is depicted in Fig. 5.6. The fit to the equation is displayed as solid lines in the same figure, while the corresponding fit parameters are presented in Table 5.3. Although the fits have been performed for two different temperature ranges ($|\tau|_{max} = 5\times10^{-3}$, 7.7×10^{-3}), the fit

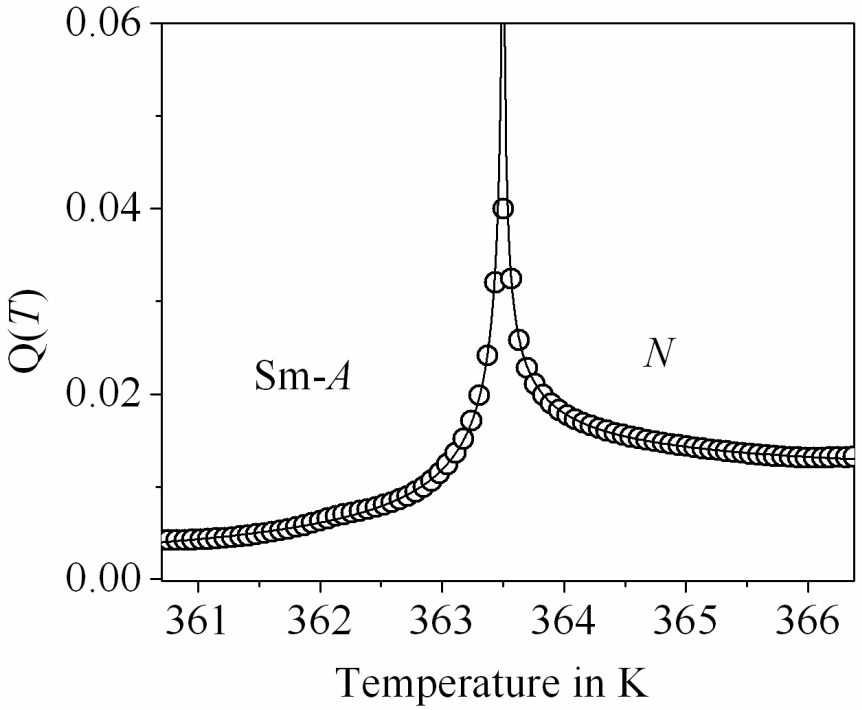

Figure 5.6. Temperature variation of the parameter Q(*T*) near the *N*–Sm-*A* phase transition for sample PhP2. Solid lines are fit to Eq. (5.2) near the *N*–Sm-*A* phase transition.

Table 5.3. Results corresponding to the best fit for Q(*T*) of pure PhP2 compound near the *N*–Sm-*A* phase transition and related χ_v^2 values associated with the fits. The *N*–Sm-*A* phase transition temperature T_{NA} = 363.5 K was kept fixed in the fits. $|\tau|_{max}$ represents the upper limit of reduced temperature considered for these fits.

Phase	α'	A^-, A^+	D^-, D^+	$\lvert\tau\rvert_{max}$	χ_v^2
Smectic-*A*	0.463±0.014	0.00057±0.00007	9.26±0.36	5×10^{-3}	1.35
Nematic	0.462±0.008	0.00035±0.00003	9.35±0.87	5×10^{-3}	1.07
Smectic-*A*	0.463±0.015	0.00073±0.00003	8.41±0.72	7.9×10^{-3}	1.06
Nematic	0.465±0.007	0.00044±0.00001	8.22±0.34	7.7×10^{-3}	1.18

range $\tau = 5\times10^{-3}$ have been accepted because the fit parameters remain practically stable for a small change in temperature range along with a minimum regular pattern in the residuals [45]. The goodness of the fits has

been tested with the help of reduced error function χ_v^2. In this study, the χ_v^2 values related to fits to the Q(T) wings are found within 1.06 and 1.35, indicating a satisfactory fit of the Q(T) data to the model expression considered. In this fits, the critical exponent α' has come out to be close to 0.462 for the pure compound PhP2 and hence indicates a nearly tricritical nature of the *N*–Sm-*A* phase transition. According to theoretical predictions, the 3D-*XY* universality class requires the occurrence of a critical amplitude ratio (A^-/A^+) equal to 0.971, a critical exponent (α') of -0.007 and (D^-/D^+) ~ 1 while for a tricritical point the critical amplitude ratio (A^-/A^+) is close to 1.6, critical exponent (α') takes on a value 0.5 and (D^-/D^+) is close to unity. Here in this case, the values of the quotients, (A^-/A^+) and (D^-/D^+) have been appeared to be 1.630±0.029 and 0.99±0.04 respectively for the fit range $\tau = 5\times10^{-3}$; both of which are also close to the tricritical values.

Investigation of the critical anomaly associated with the *N*–Sm-*A* phase transition has also been extended to the binary mixtures as well. The temperature-dependent variation of Q(T) for eight different mixtures including the pure compound PhP2 in the vicinity of *N*–Sm-*A* phase transition are depicted in Fig. 5.7 over the range $\tau = 5\times10^{-3}$. Corresponding best fitted parameters are listed in Table 5.4. The magnitude of the anomaly in Q(T) decreases significantly as the N ranges grows, showing that thermal fluctuations associated with the Q(T) anomaly are very sensitive to the saturation of nematic order parameter.

The result of fits represents the Q(T) data quite well, as indicated by the χ_v^2 values ranging between 1.02 and 1.46. However, the critical region for each mixture at the Sm-*A*–Sm-*C* phase transition is quite small compared to that for the *N*–Sm-*A* phase transition. In this study, the values of critical exponent α' has been found within 0.053 and 0.462, consequently indicating a crossover character for the *N*–Sm-*A* phase transition. Furthermore, the values of the quotients, (A^-/A^+) and (D^-/D^+) also have been appeared within a range from1.63

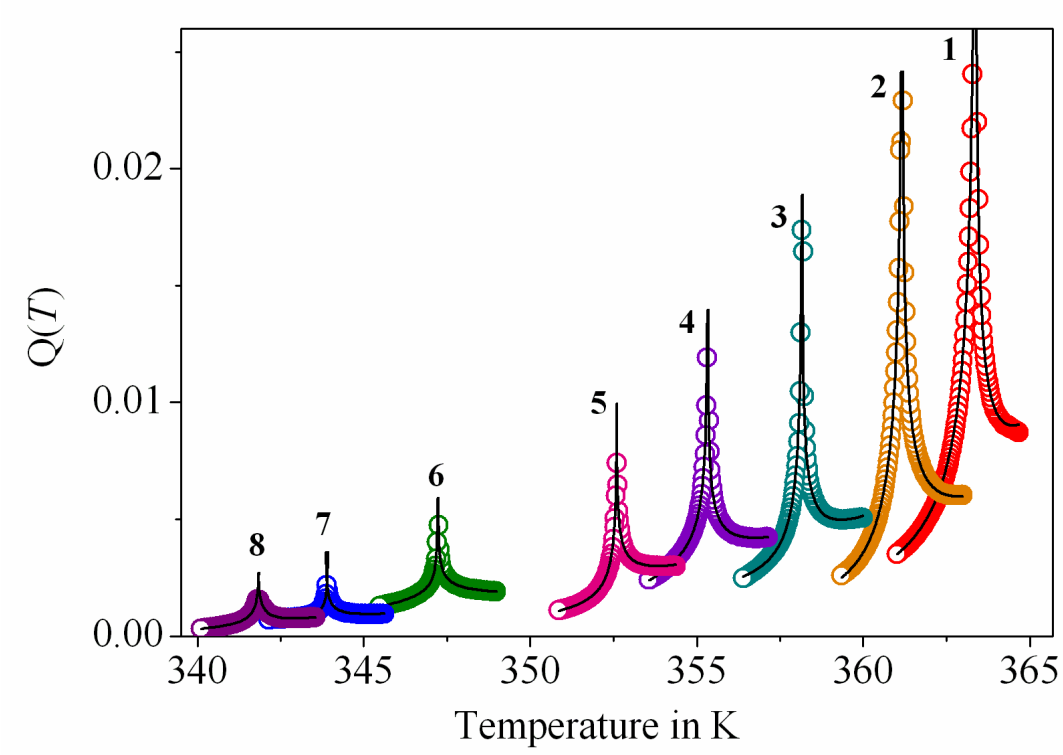

Figure 5.7. The temperature dependence of Q(*T*) in the vicinity of the *N*–Sm-*A* transition in mixtures of PhP1 and PhP2. 1: x_{PhP1} = 0.0; 2: x_{PhP1} = 0.05; 3: x_{PhP1} = 0.1; 4: x_{PhP1} = 0.15; 5: x_{PhP1} = 0.2; 6: x_{PhP1} = 0.3; 7: x_{PhP1} = 0.35; 8: x_{PhP1} = 0.4.

Table 5.4. Results corresponding to the best fit for Q(*T*) near *N*–Sm-*A* phase transition of all the mixtures obtained in accordance with Eq. (5.2) and related χ_v^2 values associated with the fits.

x_{PhP1}	A^-/A^+	D^-/D^+	α'	χ_v^2
0	1.630±0.029	0.99±0.04	0.462±0.002	1.29
0.05	1.521±0.052	0.99±0.01	0.425±0.007	1.11
0.1	1.417±0.036	1.00±0.01	0.387±0.011	1.36
0.15	1.368±0.107	1.00±0.01	0.345±0.005	1.02
0.2	1.450±0.088	1.00±0.01	0.303±0.004	1.12
0.3	1.053±0.038	1.01±0.01	0.188±0.003	1.21
0.35	0.970±0.017	1.00±0.01	0.084±0.001	1.18
0.4	0.983±0.010	1.01±0.03	0.053±0.001	1.46

to 0.97 and from 0.99 to 1.01 respectively, which reveals a well consistency with the theoretical values in between 3D-*XY* and tricritical limit. Moreover, the critical exponent α' is found to be sensitive to the temperature width of the nematic phase and exhibits a systematic variation depending on it. The variation of the critical exponent α' values for the present investigated mixtures including that for the pure PhP2 compound against the McMillan ratio ($R_M = T_{NA}/T_{IN}$) is illustrated in Fig. 5.8. Simultaneous comparison has also been displayed by placing the critical exponent values of the same mixture obtained at the Sm-*A*–Sm-*C* phase transition. It is quite evident that the theoretical value for tricritical limit is expected for a temperature ratio (R_M) of 0.87 in the vicinity of *N*–Sm-*A* phase transition, although experimental observations yields relatively higher values, ranging between 0.942 and 0.994, while for 3D-*XY*

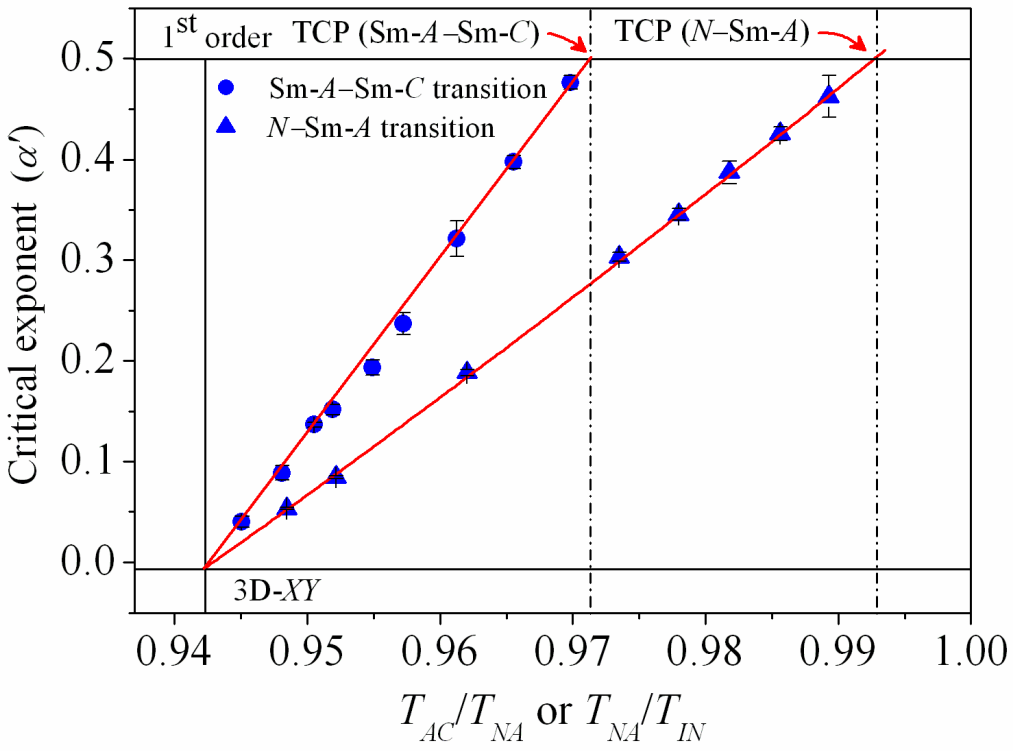

Figure 5.8. The variation of effective critical exponent (α') with T_{NA}/T_{IN} for the *N*–Sm-*A* phase transition and T_{AC}/T_{NA} for the Sm-*A*–Sm-*C* phase transition. The vertical dashed lines and solid line corresponds to the tricritical point (TCP) and 3D-*XY* limit respectively. The solid lines (red) are linear fit to the data.

limit, it is expected for a value of 0.94. In this binary system, an extrapolation of the linear fit to the extracted α' values yield a tricritical behavior (*i.e.*, $\alpha' = 0.5$) for the McMillan ratio (R_M) of 0.992, which is somewhat greater in comparison to that obtained for a similar temperature ratio $T_{AC}/T_{NA} = 0.972$ at the Sm-*A*–Sm-*C* phase transition. However, the linear fit to the α' data yields a McMillan ratio (T_{NA}/T_{IN}) value of 0.942 corresponding to the 3D-*XY* point which is found to be very close to the temperature ratio T_{AC}/T_{NA}, for the Sm-*A*–Sm-*C* phase transition. The overall behavior between α' and McMillan ratio (T_{NA}/T_{IN}) from the tricritical point (TCP) towards approaching the 3D-*XY* value is in good agreement with the previous reports on the *N*–Sm-*A* phase transitions [37,46-51]. Therefore, the origin of such critical behavior is a unique feature for the both the *N*–Sm-*A* and the Sm-*A*–Sm-*C* phase transitions for all of the compounds and they are seen to follow two distinctly different linear curves as shown in Fig. 5.8.

Based on the obtained results in present binary system confirms that the width of the *N* and Sm-*A* temperature ranges plays an important role in deciding the nature of both the *N*–Sm-*A* and the Sm-*A*–Sm-*C* phase transitions. For the appearance of a tricritical point of the *N*–Sm-*A* phase transition, it requires a nematic width around 2.5 K, while for the Sm-*A*–Sm-C phase transition the same can be obtained for a Sm-*A* range around 10.5 K. Likewise for the manifestation of 3D-*XY* limit, it requires a *N* range about 21 K for the *N*–Sm-*A* phase transition, which is nearly equal to the Sm-*A* range for the Sm-*A*–Sm-C phase transition.

5.7. Critical behavior at the *I–N* phase transition

The high resolution optical birefringence (Δn) data have also been employed to investigate the critical fluctuation appearing in vicinity of the *I–N* phase transition. In the investigated system, recourse of a four parameter power-law model [38,52,53] consistent with the mean-field theory for both critical and tricritical points of weakly first-order transitions as disscussed

earlier in chapter 3, has been adopted. According to the model, the temperature dependence of optical birefringence (Δn) in the nematic phase may be approximated as [38,54],

$$\Delta n = \zeta\,[S^{**} + (1 - S^{**})\left|1 - \frac{T}{T^{**}}\right|^{\beta} \qquad (5.3)$$

without considering any local field influence. Here, T^{**} is the temperature corresponding to the effective second order transition point and $\zeta = (\Delta\alpha/\alpha)[(n_I^2 - 1)/2n_I]$, where n_I is the refractive index in the isotropic phase (just above T_{IN}).. Thus at $T = T^{**}$, $S(T^{**}) = S^{**}$. β represents the order parameter critical exponent. This method has been appeared to be superior to the earlier attempts to fit the temperature dependence of Δn using Haller's procedure which contains a relatively smaller number of fit parameters [55]. Furthermore, the Haller's method frequently leads to relatively lower values of

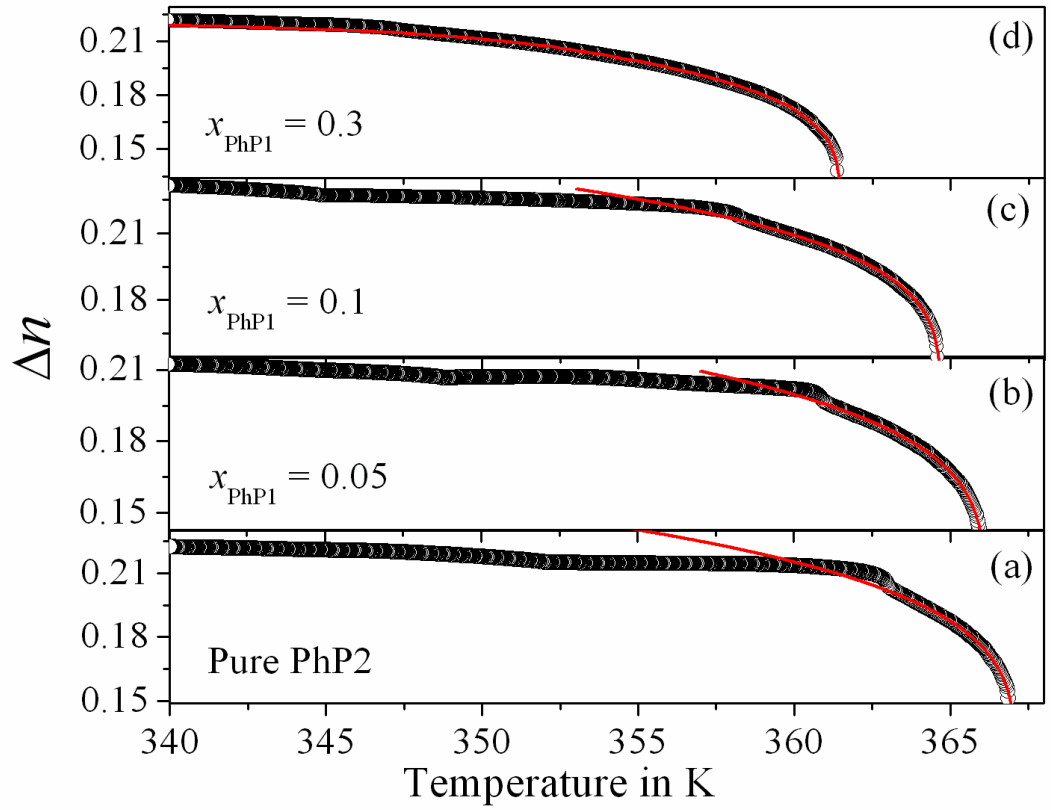

Figure 5.9. Experimental values of birefringence ($\Delta n = n_e$-n_o) as a function of temperature for (a) PhP2, (b) x_{PhP1}= 0.05, (c) x_{PhP1}= 0.1 and (d) x_{PhP1}= 0.3. Solid lines (Red) represent the fit to Eq. (5.3) and extrapolated to the Sm-*A* phase.

Table 5.5. Values of the fit parameters obtained from the four-parameter fit of the temperature dependence of Δ*n* to Eq. (5.3).

x_{PhP1}	ζ	S^{**}	T^{**} *in K*	β	T^{**}-T_{IN}	χ_v^2
0	0.390±0.071	0.28±0.22	367.07±1.77	0.248±0.208	0.24	1.04
0.05	0.364±0.049	0.29±0.16	366.09±1.37	0.248±0.161	0.35	1.09
0.1	0.368±0.025	0.34±0.08	364.65±0.81	0.249±0.091	0.18	1.13
0.15	0.391±0.142	0.29±0.43	363.66±3.64	0.251±0.428	0.32	1.11
0.2	0.372±0.049	0.27±0.16	362.31±1.34	0.251±0.156	0.22	1.27
0.3	0.349±0.005	0.32±0.02	361.46±0.21	0.251±0.023	0.33	1.01
0.35	0.367±0.007	0.33±0.02	361.21±0.25	0.251±0.027	0.25	1.40
0.4	0.308±0.009	0.42±0.04	361.01±0.51	0.251±0.052	0.21	1.39

β with $\beta \leq 0.2$ and also does not suit for its incompatibility with the weakly first-order nature of the *I–N* phase transition [56]. In the temperature dependence of birefringence a clearly distinguishable pretransitional smectic influence has been observed in a region up to few temperatures above the *N*–Sm-*A* phase transition temperature. The fits to Eq. (5.3) with the birefringence data are represented as solid line for four different mixtures in Fig. 5.9(a–d). The best fit values for the quantities Δn_0, S^{**}, T^{**} and β are listed in Table 5.5 for all of the mixtures including the pure compound PhP2. From an inspection of the extracted data it is obvious that the β value, obtained from the four parameter model expression, is clearly in line with the tricritical hypothesis (TCH) ($\beta_{TCH} = 0.25$) of Keyes [57] and Anisimov *et al.* [58,59] and thus discard the possibility of other higher theoretical values. Similar outcome has also been reported for a number of compounds with different molecular structures and also for their mixtures obtained from various experimental techniques like the specific heat capacity, birefringence, dielectric and volumetric measurements [37,38,52,53,60-66]. Hence, the present experimental outcomes once more confirm the validity of the tricritical nature for the *I–N* phase transition. Furthermore, the temperature difference (T^{**}-T_{IN}) for the pure compound PhP2

as obtained from the extracted T^{**} value is come out to be 0.24 K, which reveals a good agreement with those reported for distinct smectogenic compounds from high resolution rotating-analyzer technique [38] and refractometer measurements [52]. However, the obtained (T^{**}-T_{IN}) values for the mixtures are found to lie in a range between 0.18 to 0.35, those are comparatively higher than the reported values measured from the specific heat capacity, dielectric and molar volume measurements [61,66]. Recently from the study of the profile of the order parameter $S(T)$ derived from various anisotropic quantities, Simoes *et al.* showed that all experimental data coalesce along a common line over the entire range of the nematic phase signaling a global universal behavior [67-69]. They also obtained the critical exponent β = 0.25 together with the temperature difference (T^{**}-T_{IN}) close to 0.3. Such outcomes relating β and (T^{**}-T_{IN}) is also fairly in agreement with the present observation.

5.8. Conclusion

Precise optical birefringence measurement has been undertaken to study the Sm-*A*–Sm-*C*, *N*–Sm-*A* and *I*–*N* phase transitions in a phenyl pyrimidine (seventh homolog) liquid crystal as well as in eight binary mixtures of the same with the second homologous compound (PhP1). The precise Δn data are quite successful in probing the transitional anomaly accompanying all the phase transitions in the investigated system. No visible discontinuity appears in the temperature dependence of Δn at both the *N*–Sm-*A* and Sm-*A*–Sm-*C* phase transitions. The order character of these smectic transitions has also been explored and compared with the available theoretical models. Divergences in the quotient $Q(T)$ in the vicinity of phase transitions has been well described in terms of the renormalization-group model. For the Sm-*A*–Sm-*C* transition, a weak dependence of critical exponent α' on fit ranges has been observed for the pure compound. It is quite evident that the transitional behavior of this phase transition is really critical over the reduced temperature range 3×10^{-3}, estimated

in the range about 2 K on both side from the transition. Moreover, the non-universal values have been observed for the critical exponent α' for both the *N*–Sm-*A* and Sm-*A*–Sm-*C* phase transitions and hence indicate a crossover character from second order to the first order transition. The non-universal behavior of this transition with either very weak first-order or second-order transitions with Gaussian tricritical or crossover from 3D-*XY* critical to tricritical behavior has been clearly explained on the basis of the width of the Sm-*A* temperature range linked with the Sm-*A*–Sm-*C* phase transition, which in effect may close the controversy on the nature of the Sm-*A*–Sm-*C* transition. However, mean-field tricritical or mean-field 3D-*XY* is only an approximation where the true critical region remains inaccessible. Moreover, the origin of such critical behavior is a unique feature for the both the *N*–Sm-*A* and the Sm-*A*–Sm-*C* phase transitions for all of the compounds and they are seen to follow two distinctly different linear curves as shown in Fig. 5.8. Furthermore, for the *I–N* phase transition, the critical exponent β, characterizing the limiting behavior of the nematic order parameter close to that transition, has come out to be close to 0.25 and hence in agreement with the tricritical hypothesis. The work presented in this chapter can be useful for other temperature-driven phase transitions which include binary alloys, superconductors, ferromagnetic and ferroelectric materials, classical fluids as well as thermal phase transitions in subatomic particles [70]. Moreover, the work can also be extended to encompass all such phase transition phenomena which are not driven by temperature but also by some other parameters such as pressure, composition, or magnetic field, *i.e.*, the so-called quantum phase transitions. Particularly the recently observed phases within strongly correlated materials (viz. quantum liquid crystals) exhibiting the same symmetry breaking transitions as in classical liquid crystals which are now being intensively studied [71] and are expected to unveil a wealth of new and absorbing physics in future.

References:

[1] P.G. de Gennes, *Mol. Cryst. Liq. Cryst.*, **21,** 49 (1973).

[2] C.A. Shantz, and D.L. Johnson, *Phys. Rev. A*, **17,** 1504 (1978).

[3] C.C. Huang, and J.M. Viner, *Phys. Rev. A*, **25,** 3385 (1982).

[4] R.J. Birgeneau, C.W. Garland, A.R. Kortan, J.D. Litster, M. Meichle, B.M. Ocko, C. Rosenblatt, L.J. Yu, and J. Goodby, *Phys. Rev. A*, **27**, 1251 (1983).

[5] M. Meichle, and C.W. Garland, *Phys. Rev. A*, **27**, 2624 (1983).

[6] S.C. Lien, C.C. Huang, T. Carlsson, I. Dahl, and S.T. Lagerwall, *Mol. Cryst. Liq. Cryst.*, **108**, 149 (1984).

[7] S. Dumrongrattana, C.C. Huang, G. Nounesis, S.C. Lien, and J.M. Viner, *Phys. Rev. A*, **34**, 5010 (1986).

[8] P. Das, K. Ema, and C.W. Garland, *Liq. Cryst.*, **4**, 205 (1989).

[9] H.Y. Liu, C.C. Huang, Ch. Bahr, and G. Heppke, *Phys. Rev. Lett.*, **61**, 345 (1988).

[10] T. Chan, Ch. Bahr, G. Heppke, and C.W. Garland, *Liq. Cryst.*, **13**, 667 (1993).

[11] K. Ema, J. Watanabe, A. Takagi, and H. Yao, *Phys. Rev. E*, **52**, 1216 (1995).

[12] L. Reed, T. Stoebe, and C.C. Huang, *Phys. Rev. E*, **52**, R2157 (1995).

[13] K. Ema, A. Takagi, and H. Yao, *Phys. Rev. E*, **53**, R3036 (1996).

[14] K. Ema, M. Ogawa, A. Takagi, and H. Yao, *Phys. Rev. E*, **54**, R25 (1996).

[15] K. Ema, H. Yao, A. Fukuda, Y. Takanishi, and H. Takezoe, *Phys. Rev. E*, **54**, 4450 (1996).

[16] K. Ema, and H. Yao, *Phys. Rev. E*, **57**, 6677 (1998).

[17] D. Collin, J.L. Gallani, and P. Martinoty, *Phys. Rev. Lett.*, **61**, 102 (1988).

[18] D. Collin, S. Moyses, M.E. Neubert, and P. Martinoty, *Phys. Rev. Lett.*, **73**, 983 (1994).

[19] M. Škarabot, K. Kočevar, R. Blinc, G. Heppke, and I. Muševič, *Phys. Rev. E*, **59**, R1323 (1999).

[20] J. Fernsler, D. Wicks, D. Staines, A. Havens, and N. Paszek, *Liq. Cryst.*, **39**, 1204 (2012).

[21] C.R. Safinya, M. Kaplan, J. Als-Nielsen, R.J. Birgeneau, D. Davidov, J.D. Litster, D.L. Johnson, and M.E. Neubert, *Phys. Rev. B*, **21**, 4149 (1980).

[22] L. Benguigui, and P. Martinoty, *Phys. Rev. Lett.*, **63**, 774 (1989); *J. Phys. II France*, **7**, 225 (1997).

[23] A. Altland, and B. Simons, in *Condensed Matter Field Theory*, Cambridge University Press, Cambridge (2010).

[24] C.C. Huang, and S.C. Lien, *Phys. Rev. A*, **31**, 2621 (1985).

[25] S.K. Prasad, V.N. Raja, D.S. Rao, G.G. Nair, and M.E. Neubert, *Phys. Rev. A*, **42**, 2479 (1990).

[26] K.J. Stine, and C.W. Garland, *Phys. Rev. A*, **39**, 3148 (1989).

[27] A. Chakraborty, S. Chakraborty, and M.K. Das, *Phys. Rev. E*, **1**, 032503 (2015).

[28] L. Reed, T. Stoebe, and C.C. Huang, *Phys. Rev. E*, **52**, R2157 (1995); G.S. Iannacchione, C.W. Garland, P.M. Johnson, and C.C. Huang, *Liq. Cryst.*, **26**, 51 (1999).

[29] Y. Galerne, *Phys. Rev. A*, **24**, 2284 (1981).

[30] K. Ema, and H. Yao, *Phys. Rev. E*, **57,** 6677 (1998), and reference therein.

[31] A. Chakraborty, S. Chakraborty, and M.K. Das, *Physica B*, **479**, 90 (2015).

[32] M.K. Das, S. Chakraborty, R. Dabrowski, and M. Czerwinski, *Phys. Rev. E*, **95**, 012705 (2017).

[33] A. Saipa, and F. Giesselmann, *Liq. Cryst.*, **29**, 347 (2002).

[34] G. Sarkar, M.K. Das, R. Paul, B. Das, and W. Weissflog, *Phase Transit.*, **82**, 433 (2009).

[35] T. Scharf, in *Polarized Light in Liquid Crystals and Polymers*, Wiley, Hoboken, NJ (2007).

[36] A. Prasad, and M.K. Das, *J. Phys.: Condens. Matter*, **22**, 195106 (2010).

[37] A. Chakraborty, S. Chakraborty, and M.K. Das, *Phys. Rev. E*, **91**, 032503 (2015).

[38] S. Erkan, M. Çetinkaya, S. Yildiz, and H. Özbek, *Phys. Rev. E*, **86**, 041705 (2012); and references therein.

[39] H.E. Stanley, in *Introduction to Phase Transitions and Critical Phenomena*, Clarendon, Oxford (1971).

[40] R. Brout, in *Phase Transitions*, Benjamin, New York, (1965).

[41] M.C. Cetinkaya, S. Yildiz, H. Ozbek, P. Losada-Perez, J. Leys, and J. Thoen, *Phys. Rev. E*, **88**, 042502 (2013).

[42] P.R. Bevington, and D.K. Robinson, in *Data Reduction and Error Analysis for the Physical Sciences (3rd ed.)*, McGraw-Hill, New York (2003).

[43] K. Ema, H. Yao, T. Matsumoto, and A. Fukuda, *Mol. Cryst. Liq. Cryst.*, **364**, 335 (2001).

[44] M. E. Fisher, *Phys. Rev.*, **176**, 257 (1968).

[45] J.A. Potton, and P.C. Lanchester, *Phase Transit.*, **6**, 43 (1985).

[46] S.K. Sarkar, and M.K. Das, *J. Mol. Liq.*, **199**, 415 (2014).

[47] S.K. Sarkar, A. Chakraborty, and M.K. Das, *Liq. Cryst.*, **43**, 22 (2016).

[48] S. Chakraborty, A. Chakraborty, and M.K. Das, *J. Mol. Liq.*, **219**, 608 (2016).

[49] G. Cordoyiannis, C.S.P. Tripathi, C. Glorieux, and J. Thoen, *Phys. Rev. E*, **82**, 031707 (2010).

[50] C.W. Garland, and G. Nounesis, *Phys. Rev. E*, **49**, 2964 (1994).

[51] Y. Sasaki, K. Ema, K.V. Le, H. Takezoe, S. Dhara, and B.K. Sadashiva, *Phys. Rev. E*, **83**, 061701 (2011).

[52] I. Chirtoc, M. Chirtoc, C. Glorieux, and J. Thoen, *Liq. Cryst.*, **31**, 229 (2004).

[53] S. Yildiz, H. Özbek, C. Glorieux, and J. Thoen, *Liq. Cryst.*, **34**, 611 (2007).

[54] H. Ozbek, S. Ustunel, E. Kutlu, and M.C. Cetinkaya, *J. Mol. Liq.*, **199**, 275 (2014).

[55] I. Haller, *Progr. Solid State Chem.*, **10**, 103 (1975).

[56] J. Thoen, and G. Menu, *Mol. Cryst. Liq. Cryst.*, **97**, 163 (1983).

[57] P.H. Keyes, *Phys. Lett. A*, **67**, 132 (1978).

[58] M.A. Anisimov, S.R. Garber, V.S. Esipov, V.M. Mamnitskii, G.I. Ovodov, L.A. Smolenko, and E.L. Sorkin, *Sov. Phys. JETP*, **45**, 1042 (1977).

[59] M.A. Anisimov, *Mol. Cryst. Liq. Cryst.*, **162A**, 1 (1988).

[60] S.K. Sarkar, P.C. Barman, and M.K. Das, *Physica B*, **446**, 80 (2014).

[61] P. Cusmin, M.R. de la Fuente, J. Salud, M.A. Pérez-Jubindo, S. Diez-Berart, and D.O. López, *J. Phys. Chem. B*, **111**, 8974 (2007).

[62] J. Salud, P. Cusmin, M.R. de la Fuente, M.A. Pérez-Jubindo, D.O. López, and S. Diez-Berart, *J. Phys. Chem. B*, **113**, 15967 (2009).

[63] A. Drozd-Rzoska, S.J. Rzoska, and J. Zioło, *Phys. Rev. E.*, **54**, 6452 (1996).

[64] S.J. Rzoska, J. Ziolo, W. Sulkowski, J. Jadżyn, and G. Czechowski, *Phys. Rev. E.*, **64**, 052701 (2001).

[65] A. Prasad, and M.K. Das, *Phys. Scr.*, **84**, 015603 (2011).

[66] A. Żywociński, *J. Phys. Chem. B.*, **107**, 9491 (2003).

[67] M. Simões, and D.S. Simeão, *Phys. Rev. E.*, **74**, 051701 (2006).

[68] M. Simões, D.S. Simeão, and K.E. Yamaguti, *Liq. Cryst.*, **38**, 935 (2011).

[69] M. Simões, D.S. Simeão, and S.M. Domiciano, *Mol. Cryst. Liq. Cryst.*, **576**, 76 (2013).

[70] Y. Hidaka, and S. Kai, *Forum Forma*, **24**, 123 (2009).

[71] P. Romanczuk, H. Chaté, L. Chen, S. Ngo, and J. Toner, *New J. Phys.*, **18,** 063015 (2016).